

Automated Ensemble-Based Segmentation of Pediatric Brain Tumors: A Novel Approach Using the CBTN-CONNECT-ASNR-MICCAI BraTS-PEDs 2023 Challenge Data

Shashidhar Reddy Javaji^{1*}, Sovesh Mohapatra^{1,2*}, Advait Gosai¹, Gottfried Schlaug^{2,3,4#}

¹Manning College of Information and Computer Sciences, University of Massachusetts Amherst, MA

²Institute for Applied Life Sciences, University of Massachusetts Amherst, MA

³Department of Biomedical Engineering, University of Massachusetts Amherst, MA

⁴Department of Neurology, Baystate Medical Center, and UMass Chan Medical School - Baystate Campus, Springfield, MA.

*contributed equally

#corresponding author

Corresponding author: E-mail: gschlaug@umass.edu;

Abstract:

Brain tumors remain a critical global health challenge, necessitating advancements in diagnostic techniques and treatment methodologies. In response to the growing need for age-specific segmentation models, particularly for pediatric patients, this study explores the deployment of deep learning techniques using magnetic resonance imaging (MRI) modalities. By introducing a novel ensemble approach using ONet and modified versions of UNet, coupled with innovative loss functions, this study achieves a precise segmentation model for the BraTS-PEDs 2023 Challenge. Data augmentation, including both single and composite transformations, ensures model robustness and accuracy across different scanning protocols. The ensemble strategy, integrating the ONet and UNet models, shows greater effectiveness in capturing specific features and modeling diverse aspects of the MRI images which result in lesion-wise dice scores of 0.52, 0.72 and 0.78 for enhancing tumor, tumor core and whole tumor labels respectively. Visual comparisons further confirm the superiority of the ensemble method in accurate tumor region coverage. The results indicate that this advanced ensemble approach, building upon the unique strengths of individual models, offers promising prospects for enhanced diagnostic accuracy and effective treatment planning for brain tumors in pediatric brains.

1. Introduction:

Brain tumor has been a major global health challenge, impacting not only adults but also children and adolescents¹. In 2022, the United States alone reported an estimated 40,594 individuals, from infancy to 19 years of age, diagnosed with primary brain or other central nervous system (CNS) tumors. Among these, pilocytic astrocytoma was the predominant histopathologic group, accounting for 8,264 cases. Given that survival rates following a diagnosis are particularly low among infants, there is a huge need to develop age-specific segmentation models². These models could enable precise and automated detection of tumor regions within pediatric brains, thereby facilitating more efficient and fast diagnosis and treatment.

With the increasing use of deep learning techniques in conjunction with different modalities of MRI, different models, especially the U-shaped architectures, have demonstrated precise and accurate performance across various medical image segmentation tasks³⁻⁵. Various models have been employed for whole brain segmentation, yet certain architectural designs have been observed to perform better in segmenting specific regions within the brain⁶. This phenomenon can be attributed to the intricate relationship between the complexities inherent in both the architecture and the brain's structure. Just as different modalities provide complementary information about anomalous regions in the brain, different architectures may be more adept at handling particular areas of the brain.

In this paper, we are focused on using the CBTN-CONNECT-DIPGr-ASNR-MICCAI BraTS-PEDs 2023 Challenge data which constitutes four different modalities (native T1, post-contrast T1-weighted (T1Gd), T2-weighted (T2), and T2 Fluid Attenuated Inversion Recovery (T2-FLAIR))⁷. We introduce a novel ensemble approach using ONet and various modified versions of UNet along with modified loss functions which yielded a more precise segmentation for the pediatric tumors.

2. Methodology

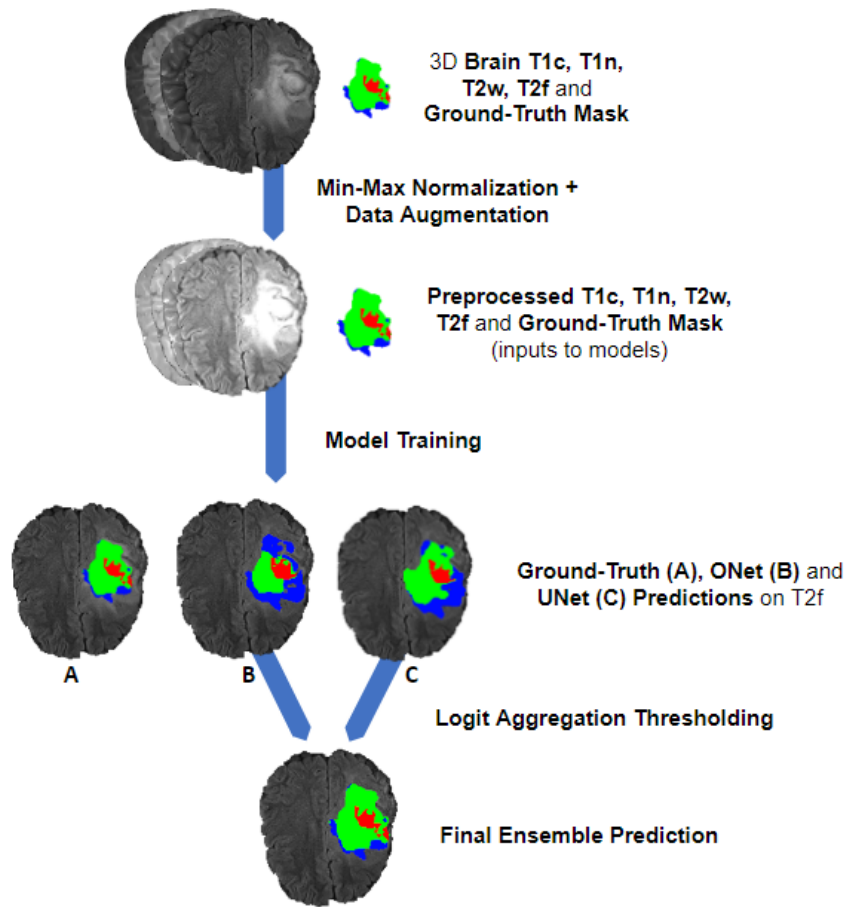


Figure - 1. Comprehensive workflow – visualizing the end-to-end process with model training and ensembling approaches

2.1. Data Augmentation

Due to the inherent variability and noise that can occur during acquisition using different scanners, the integration of various physics-inspired augmentation techniques is essential. By populating the training data with these techniques, the model becomes robust and accurate across diverse scanning protocols.

In this study, we used two different approaches of augmentation: single and composite transformation. For the single transformation, we used techniques like flip, affine transformation, elastic deformation, noise, rescale Intensity, and random bias field. Additionally, in composite transformation, a combination of some or all of the aforementioned techniques was applied to further enrich the dataset.

2.2. Model Architectures

In this work, we implemented eight unique variations using two fundamental base architectures, each paired with different loss functions (further explained in section 2.3) and tailored hyperparameters. Figure - 2 illustrates the architecture for one of the variants of the UNet3D configurations.

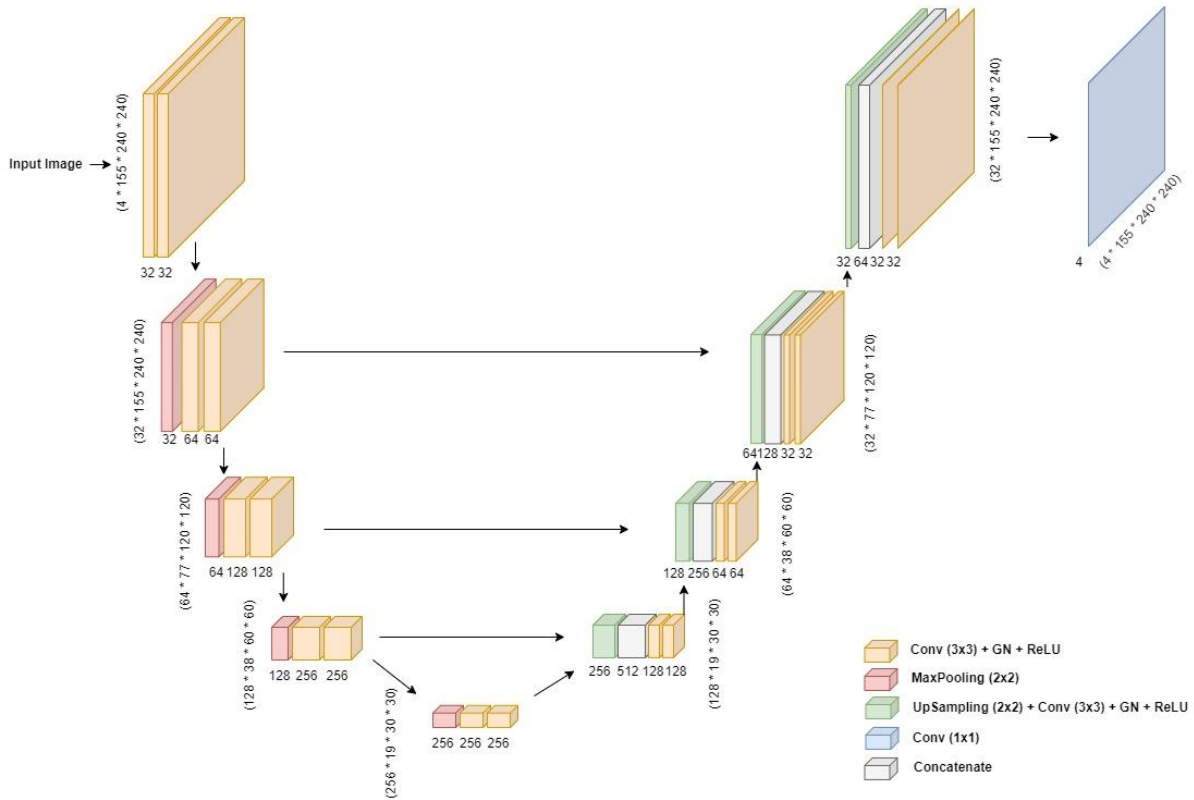


Figure - 2. Core UNet3D Architecture

Listed below are the different variations applied to the fundamental base architecture of UNet3D model:

1. **3D UNet:** UNet3d(in_channels = 4, n_classes = 3, n_channels = 32).
2. **3D UNet GELU:** UNet3dGELU(in_channels=4, n_classes=3, n_channels=32). 3DUNet with all ReLU replaced by GELU activation function.
3. **3D UNet SingleConv:** UNet3dSingleConv(in_channels=4, n_classes=3, n_channels=32). 3DUNet with single convolution instead of double convolution per upscale/downscale.
4. **3DUnet Attention:** UNet3dAtten(in_channels=4, n_classes=3, n_channels=32). 3DUNet with an attention layer.
5. **3DUnet Dropout:** UNet3dDropout(in_channels=4, n_classes=3, n_channels=32), 3D UNet with application of Dropout

2.1.2. ONet3D Family

Below are the different variations applied to the fundamental base architecture of ONet3D where the encoder-decoder sections are concatenated before the output convolution layer:

1. **3D ONet SingleConv Kernel_1**: ONet3DSingleConv1(in_channels=4, n_classes=3, n_channels=32, kernel_size = 1)
2. **3D ONet SingleConv Kernel_5**: ONet3DSingleConv5(in_channels=4, n_classes=3, n_channels=32, kernel_size = 5)
3. **3D ONet DoubleConv Kernel_1**: ONet3DDoubleConv1(in_channels=4, n_classes=3, n_channels=32, kernel_size = 1)

2.3. Loss Functions

In our segmentation framework, we explored different loss functions to optimize the model performance. Specifically, we employed two distinct loss combinations: Binary Cross-Entropy (BCE) plus Dice Loss, and Generalized Dice Loss plus BCE. The choice of these loss functions is motivated by their abilities to tackle the class imbalance problem often encountered in medical image segmentation.

2.3.1. Binary Cross-Entropy combined with Dice Loss

The Binary Cross-Entropy (BCE) loss is commonly used for binary classification tasks and computes the cross-entropy between the true labels and predicted probabilities. To enhance the model's sensitivity to the region of interest, we combined BCE with Dice Loss. The Dice Loss computes the overlap between the predicted segmentation and the ground truth, providing a spatially aware metric that is sensitive to the shape of the segmented structures.

$$\text{BCE}(y, \hat{y}) = -\frac{1}{N} \sum_{i=1}^N (y_i \log(\hat{y}_i) + (1 - y_i) \log(1 - \hat{y}_i))$$

$$\text{Dice}(y, \hat{y}) = 1 - \frac{2 \sum_{i=1}^N y_i \hat{y}_i + \epsilon}{\sum_{i=1}^N y_i + \sum_{i=1}^N \hat{y}_i + \epsilon}$$

$$\text{Loss}(y, \hat{y}) = \alpha \cdot \text{BCE}(y, \hat{y}) + \beta \cdot \text{Dice}(y, \hat{y})$$

2.3.2. Generalized Dice Loss combined with BCE

Recognizing the limitations of standard Dice Loss in handling cases with varying object sizes, we also experimented with Generalized Dice Loss (GDL). GDL extends the traditional Dice Loss by incorporating class-wise weights, thus accommodating the imbalanced class distribution. This loss function is especially well-suited to medical image segmentation where certain classes or labels may be underrepresented.

$$\text{GDL}(y, \hat{y}) = 1 - \frac{2 \sum_{c=1}^C w_c \sum_{i=1}^N y_{ci} \hat{y}_{ci} + \epsilon}{\sum_{c=1}^C w_c \left(\sum_{i=1}^N y_{ci} + \sum_{i=1}^N \hat{y}_{ci} \right) + \epsilon}$$

$$w_c = \frac{1}{\left(\sum_{i=1}^N y_{ci}\right)^2}$$

2.4. Ensemble Strategy

The ensemble strategy integrates the predictive capabilities of ONet and UNet models, capitalizing on their complementary strengths. Initial predictions from the models are combined through a summation of logits, followed by thresholding. A majority vote across the models for each voxel finalizes the ensemble prediction, aiming to capture specific features and model diverse aspects of the MRI images.

2.5. Post Processing

Post-processing techniques are applied to the combined predictions to refine segmentation quality:

1. Size Filtering Based on Voxel Volumes: This technique removes small isolated regions, eliminating noise.
2. Morphological Reconstruction: A more advanced method for interpolation of voxels violating constraints and smoothing boundaries for all labels.

3. Results

3.1. Evaluation Metrics

The BraTS challenge evaluates submitted models using two primary metrics: the lesion-wise Dice score and the 95th percentile lesion-wise Hausdorff distance (HD95). These metrics are used to assess segmentations across three distinct tumor sub-regions: the whole tumor, core tumor, and active tumor.

3.1.1 Lesion-wise Dice Score:

The Dice score fundamentally measures the spatial overlap between the predicted segmentations and the actual ground truth. In the context of lesion-wise assessment, the Dice score is calculated for each individual lesion or component. The score ranges from 0 to 1, where 0 indicates no overlap and 1 represents perfect agreement between the predicted and true segmentations. For this particular method, all False Positives and False Negatives are penalized by assigning a 0 score for the Dice metric. Then, the mean Dice score is computed using given case IDs.

3.2.1. 95th Percentile Lesion-wise Hausdorff Distance (HD95):

The Hausdorff distance provides a measurement of the greatest of all the distances from a point in one set to the closest point in the other set. Essentially, it quantifies how much the predicted and ground truth segmentations deviate from each other. In the lesion-wise context, the HD95 scores are calculated for each lesion or component. False Positives and False Negatives are assigned a specific value of 374 for the HD95 metric, introducing a penalization process that influences the overall evaluation. Finally, the mean HD95 is computed using given case IDs.

Together, these metrics facilitate a comprehensive and precise evaluation of the model's segmentation ability, reflecting both the degree of overlap with the ground truth and the magnitude of deviation. By considering individual lesions, the analysis becomes more refined, enabling a deeper understanding of how well the model is performing at the localized level, and therefore allowing for more targeted improvements in future iterations.

3.2. Quantitative Performance

Table - 1: Comparison of different evaluation metrics for enhancing tumor

Models	Lesion_wise Dice	Dice	Lesion_wise Hausdorff95	Hausdorff95
UNet3D	0.43	0.44	168.68	114.03
ONet3D	0.52	0.48	131.28	121.74
Ensemble_BCE and Dice Loss	0.38	0.38	186.73	141.84
Ensemble_BCE and GD Loss	0.52	0.49	127.11	105.46

Table - 2: Comparison of different evaluation metrics for Tumor Core

Models	Lesion_wise Dice	Dice	Lesion_wise Hausdorff95	Hausdorff95
UNet3D	0.70	0.75	44.68	12.19
ONet3D	0.71	0.74	33.26	19.82
Ensemble_BCE and Dice Loss	0.64	0.73	60.00	17.68
Ensemble_BCE and GD Loss	0.72	0.74	23.84	11.48

Table - 3: Comparison of different evaluation metrics for Whole Tumor

Models	Lesion_wise Dice	Dice	Lesion_wise Hausdorff95	Hausdorff95
UNet3D	0.75	0.82	45.51	11.85
ONet3D	0.76	0.80	32.88	19.31
Ensemble_BCE and Dice Loss	0.70	0.82	61.74	15.97
Ensemble_BCE and GD Loss	0.78	0.82	25.88	10.89

In our assessment of various models, we submitted the results to the synapse portal for testing the results on the validation. The findings revealed that the ensemble training approach demonstrates better effectiveness in comparison to the single model training approach, across almost all of the validation cases.

Furthermore, an individual evaluation of predictions indicated that the single-model training approach of the ONet3D model matches the ensemble training approach for lesion_wise dice as outlined in Table 1. This indicates that there can be an ensemble model which might be robust and be generalizable for a larger dataset. However for specific types of segmentation and evaluation metrics, the approaches might differ.

3.3. Visual Comparison

Figure - 3 illustrates a side-by-side comparison of prediction results derived from two separate methodologies for modeling: individual model training and the ensemble approach.

The comparison reveals a noticeable difference between the two approaches. The predictions stemming from the single model training method, as evidenced by UNet3D and ONet3D, demonstrate to capture less core tumor region and region affected by the tumor (enhancing tumor). This limitation is contrasted by the predictions generated through the ensemble training method.

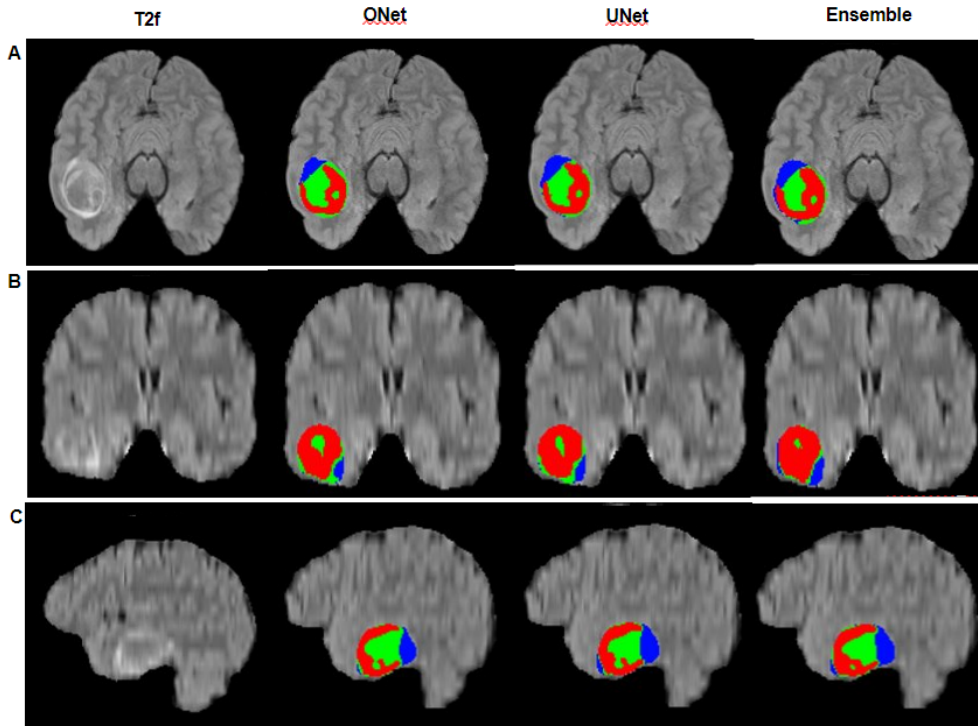


Figure - 3. A, B, and C depict three slice planes (sagittal, coronal, axial) from the same CaseID, showcasing predictions generated by three different models—UNet3D, ONet3D, and the ensemble model respectively.

The ensemble approach adds the strengths of multiple individual models, potentially leading to more accurate and robust predictions. In the context of the figure, it becomes evident that employing the ensemble method results in more effective coverage of tumor regions. This might suggest that the ensemble training not only compensates for the limitations observed in the single model training but possibly enhances the overall predictive capability.

4. Discussion and Conclusion

The integration of ONet and UNet models through an ensemble technique, together with the novel proposed post-processing strategy, creates an advanced approach to medical image segmentation. This method builds upon the unique strengths of both ONet and UNet models, combining them in an interdependent manner that leverages their individual capabilities. By doing so, the approach not only amplifies the robustness of the segmentation but also adds a level of precision that might be unattainable with a single-model training strategy. The clinical significance of this methodology lies in its potential to offer enhanced diagnostic accuracy and effective treatment planning.

5. References

1. Mackay, A. *et al.* Integrated Molecular Meta-Analysis of 1,000 Pediatric High-Grade and Diffuse Intrinsic Pontine Glioma. *Cancer Cell* **32**, 520–537.e5 (2017).
2. Ostrom, Q. T., Price, M., Ryan, K., Edelson, J. & Neff, C. CBTRUS statistical report: pediatric brain tumor foundation childhood and adolescent primary brain and other central nervous system tumors diagnosed in the United *Neuro* (2022).
3. Ronneberger, O., Fischer, P. & Brox, T. U-Net: Convolutional Networks for Biomedical Image Segmentation. in *Medical Image Computing and Computer-Assisted Intervention – MICCAI 2015* 234–241 (Springer International Publishing, 2015).
4. Hatamizadeh, A. *et al.* Swin UNETR: Swin Transformers for Semantic Segmentation of Brain Tumors in MRI Images. in *Brainlesion: Glioma, Multiple Sclerosis, Stroke and Traumatic Brain Injuries* 272–284 (Springer International Publishing, 2022).
5. Heiliger, L. *et al.* AutoPET Challenge: Combining nn-Unet with Swin UNETR Augmented by Maximum Intensity Projection Classifier. *arXiv [eess.IV]* (2022).
6. Mohapatra, S. *et al.* Meta-Analysis of Transfer Learning for Segmentation of Brain Lesions. *arXiv [eess.IV]* (2023).
7. Kazerooni, A. F. *et al.* The Brain Tumor Segmentation (BraTS) Challenge 2023: Focus on Pediatrics (CBTN-CONNECT-DIPGR-ASNR-MICCAI BraTS-PEDs). *ArXiv* (2023).